Available online at www.sciencedirect.com
ScienceDirect
Journal of Catalysis 249 (2007) 195–207
JOURNAL OF CATALYSIS
www.elsevier.com/locate/jcat

# Conversion of methanol to hydrocarbons over zeolite H-ZSM-5: On the origin of the olefinic species

Morten Bjørgen [a,*], Stian Svelle [b], Finn Joensen [a], Jesper Nerlov [a], Stein Kolboe [b], Francesca Bonino [c], Luisa Palumbo [c], Silvia Bordiga [c], Unni Olsbye [b]

[a] *Haldor Topsøe A/S, Nymøllevej 55, DK-2800 Lyngby, Denmark*
[b] *Center for Materials Science and Nanotechnology, Department of Chemistry, University of Oslo, P.O. Box 1033 Blindern, N-0315 Oslo, Norway*
[c] *Department of Inorganic, Physical and Materials Chemistry, NIS Centre of Excellence, and Centro di Riferimento INSTM, University of Turin, Via P. Giuria 7, I-10125 Torino, Italy*

Received 22 February 2007; revised 21 March 2007; accepted 9 April 2007

Available online 5 June 2007

**Abstract**

This study examined the reaction mechanism with respect to both catalyst deactivation and product formation in the conversion of methanol to hydrocarbons over zeolite H-ZSM-5. The reactivity of the organics residing in the zeolite voids during the reaction was assessed by transient $^{12}C/^{13}C$ methanol-switching experiments. In contrast to previously investigated catalysts (H-SAPO-34 and H-beta), hexamethylbenzene is virtually unreactive in H-ZSM-5 and is thus not a relevant reaction intermediate for alkene formation. However, the lower methylbenzenes are reaction intermediates in a hydrocarbon pool-type mechanistic cycle and are responsible for the formation of ethene and propene. An additional reaction cycle not applicable for ethene also must be taken into account. The $C_{3+}$ alkenes are to formed through rapid alkene methylation and cracking steps to a considerable extent; thus, methanol is converted to hydrocarbons according to two catalytic cycles over H-ZSM-5. Moreover, in contrast to what occurs for large-pore zeolites/zeotypes, molecules larger than hexamethylbenzenes are not built up inside the H-ZSM-5 channels during deactivation. Thus, deactivation is explained by coke formation on the external surface of the zeolite crystallites only. This is a plausible rationale for the superior lifetime properties of H-ZSM-5 in the methanol-to-hydrocarbon reaction.


*Keywords:* ZSM-5; MFI; MTO; MTH; MTG; Methanol; Zeolite; Mechanism; Hydrocarbon pool; Coking; Deactivation

## 1. Introduction

The current pricing of crude oil has led to increased interest in the use of natural gas or coal as a feedstock for the production of gasoline and petrochemicals. Methanol can be made from such feedstocks via synthesis gas and further converted into gasoline-range hydrocarbons or alternatively light, possibly polymer-grade alkenes. The zeolite-catalyzed conversion of methanol to hydrocarbons is commonly referred to as the MTH reaction, but because process conditions and catalyst choice alter product selectivity, the abbreviations MTO (methanol to olefins) and MTG (methanol to gasoline) are frequently used depending on the desired products.

The MTH chemistry and its commercial potential have been known for decades. The energy crisis in the 1970s sparked new interest in MTG technology. In the late 1970s, the New Zealand government decided to build the world's first facility for producing gasoline from natural gas via methanol [1]. In 1986, a plant with a planned annual gasoline production of 600,000 tons over a H-ZSM-5 catalyst was started up, but, due to the subsequent drop in crude oil prices, only the methanol synthesis step was left on stream. The Topsøe integrated gasoline synthesis (TIGAS) process of Haldor Topsøe AS, also based on H-ZSM-5 as the catalyst, was demonstrated on a pilot scale in the mid-1980s [2]. However, the TIGAS process was never scaled up due to the situation in the global energy market. Later, more attention was paid to the MTO reaction, and the manufacturing of polymer-grade ethene and propene from methanol using the UOP/Norsk Hydro technology was demonstrated in a demo

* Corresponding author.
*E-mail address:* mobj@topsoe.dk (M. Bjørgen).

0021-9517/$ – see front matter 
doi:10.1016/j.jcat.2007.04.006

plant [3]. The catalyst choice for the UOP/Norsk Hydro MTO process is the silicoaluminophosphate H-SAPO-34. Lurgi developed a process specifically aiming at selectively converting methanol into propene (MTP) over H-ZSM-5, and the process was demonstrated in a joint Lurgi/Statoil demo plant.

Today, commercial interest in MTG is again increasing, and activities involving both natural gas and coal as feedstocks are emerging. New-generation methanol plants designed to produce larger amounts of product at significantly lower cost are due to come online within the next 5 years, which will increase the profit and interest in methanol downstream activities.

Over the years, the complex mechanism of the MTH reaction has posed a challenge to catalysis investigators. In a simplified route of the MTH reaction, methanol is dehydrated under formation of dimethyl ether and water, followed by formation of alkenes from this equilibrium mixture of oxygenates. The long-standing question has been the specific mechanism behind this latter step, in which C–C bonds are formed from oxygenates (methanol/dimethyl ether). There is presently strong evidence disfavoring direct mechanisms in which methanol/dimethyl ether molecules are combined to form, for example, ethene during steady-state conversion [4–6]. Hunger and co-workers [7,8] have published data indicating that a direct route from methanol/dimethyl ether to hydrocarbons may operate during an induction period. However, this direct route most likely operates at a rate so low as to be eclipsed by even trace impurities of higher alcohols/hydrocarbons in the methanol feed, the catalyst, or the carrier gas.

On the other hand, an all-dominating indirect route known as the "hydrocarbon pool mechanism" has been gradually accepted in recent years. The hydrocarbon pool mechanism was conceptually introduced by Dahl and Kolbe in the early 1990s [9,10], and more recent independent contributions [11–24], have led to an in-depth description of the MTH reaction mechanism. The hydrocarbon pool has been described as a catalytic scaffold composed of larger organic molecules adsorbed in the zeolite to which methanol/dimethyl ether is added and from which alkenes and water are formed in a closed cycle, in which high-energy intermediates are avoided.

The identity and the operation of the hydrocarbon pool have been fairly well described for some specific systems, in particular zeolite H-beta [16–21] and H-SAPO-34 [13–15]. For these catalysts, the hydrocarbon pool has been identified as highly methyl-substituted benzene rings ("polymethylbenzenes") or the benzenium cations derived thereof. In the wide pore beta zeolite, the terminal benzene methylation product (i.e., the heptamethylbenzenium cation) is unquestionably the species responsible for the major part of alkene formation. According to the hydrocarbon pool mechanism over the beta zeolite, the heptamethylbenzenium cation splits off (at least) propene and butene under a concomitant formation of the tetra- and trimethylbenzenium ions, respectively. The heptamethylbenzenium cation is then reformed by subsequent methylation of these lower polymethylbenzenium ions (after deprotonation) by methanol/dimethyl ether, thus completing the cycle. A simplified representation of this reaction cycle is outlined in Scheme 1. The hexaMB plays a similar role in H-SAPO-34.

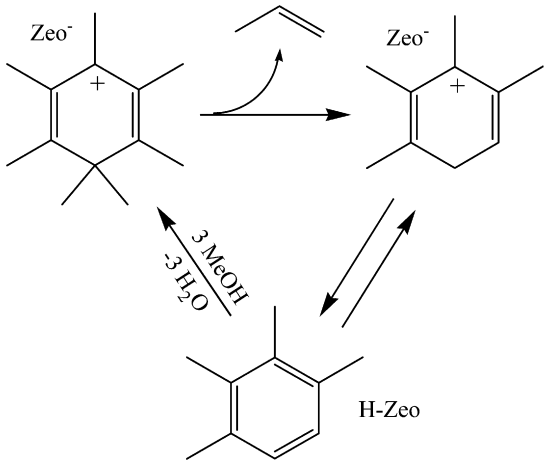


Scheme 1. Suggested hydrocarbon pool mechanism for propene formation from the heptamethylbenzenium cation over zeolite H-beta.

To date, the most extensive fundamental mechanistic understanding has been attained for the H-SAPO-34 and H-beta catalysts, and many aspects may vary with, for example, pore architecture and also possibly catalyst acidic strength/density. In the present contribution, the mechanism of the MTH reaction over H-ZSM-5, the archetype MTH catalyst, was pursued. Main attention was given to the buildup and reactivity of the organics trapped within the zeolite voids. This work demonstrates that the reaction scheme for alkene formation from methanol over H-ZSM-5 is different than those drawn previously for H-beta and H-SAPO-34. In addition to a modified hydrocarbon pool mechanism, wherein ethene is formed from the lower methylbenzenes, a parallel $C_{3+}$ alkene methylation/cracking cycle is operative. We mentioned this latter property in a recent communication [25]; the present work supplements this with more extensive data and a more thorough discussion.

## 2. Experimental

### 2.1. Catalyst and catalyst characterization

A commercially available H-ZSM-5 (Si/Al = 140) from Zeolyst International was used in this study. Powder X-ray diffraction (XRD) was performed in Bragg-Brentano parafocusing geometry using a Philips X'Pert Pro vertical T-T diffractometer and Cu$K\alpha$ radiation. The FTIR transmission spectra were collected using a cryogenic cell allowing high-temperature treatment of the sample in vacuum. The sample was pretreated at 500 °C for 1 h and kept at −213 °C during the subsequent CO adsorption/desorption. A detailed description of the cryogenic cell (consisting of a modified closed-circuit liquid He Oxford CCC 1204 cryostat) is available elsewhere [26]. The spectra were acquired at a resolution of 1 $cm^{-1}$ by averaging 128 interferograms on a Bruker Equinox-55 FTIR spectrometer. The BET surface area was obtained from a Quantachrome Autosorb by $N_2$ adsorption at −196 °C. The sample was outgassed at 350 °C for 18 h before the $N_2$ adsorption measurement.

### 2.2. Catalytic studies

The catalytic reactions were carried out in a fixed-bed Pyrex reactor using 60 mg of catalyst. The catalyst powder was compressed to wafers that were crushed and sieved to obtain 0.25–0.42 mm particles. The reaction temperature, measured using a thermocouple inserted in the catalyst bed, was between 290 and 390 °C. Methanol, either $^{13}$C-enriched (Cambridge Isotope Laboratories, 99% $^{13}$C purity) or ordinary $^{12}$C methanol (BDH Laboratory Supplies, >99.8% chemical purity) was fed by passing a He carrier gas stream, maintained at 35 mL min$^{-1}$, through a saturation evaporator kept at 20 °C. The resulting feed partial pressure was 130 hPa, giving a feed rate (WHSV) of 7.0 g g$^{-1}$ h$^{-1}$.

Three types of experiments were performed in the mechanistic investigation:

1. Ordinary $^{12}$C methanol was reacted for predetermined times at given reaction temperatures. Effluent analyses were performed during the reaction, and analyses of the organic material retained in the zeolite (see below) were carried out after each run.
2. Alternatively, the methanol feed was stopped after a given time by bypassing the evaporator and flushing the catalyst with carrier gas at the reaction temperature for a set time, followed by analysis of the retained material.
3. Using two separate and identical feed lines, it was possible to switch from $^{12}$C to $^{13}$C methanol without otherwise disrupting the experimental conditions. The isotopic compositions of both effluent compounds and retained material were determined at increasing $^{13}$C methanol reaction times (see Section 3.2.5).

#### 2.2.1. Analysis of organic material retained in the zeolite

After the catalyst sample was removed from the reactor and rapidly cooled to room temperature, a part of the catalyst mass (40 mg) was transferred to a screw-cap Teflon vial and dissolved in 1.0 mL of 15% HF. Acid treatment for 1 h was sufficient to dissolve the catalyst completely; further increases treatment time did not change the results. Then 1.0 mL $CH_2Cl_2$ (Fluka puriss) was added to the solution thus obtained to extract the liberated organic molecules from the aqueous phase. After 15 min, the organic phase and the water phase were separated, and the $CH_2Cl_2$ extract was analyzed using a gas chromatograph with a mass sensitive detector (GC–MS). The technique of dissolving the zeolite crystals in HF to recover confined constituents by extraction has been used previously in related studies [14,15,18,21,25,27] and was introduced by Guisnet et al. [28].

#### 2.2.2. Chromatography

The reactor effluent was analyzed quantitatively by online GC (Carlo Erba, GC6000-Vega series 2, with a flame ionization detector) with a Supelco SPB-5 column (60 m, 0.53 mm i.d., stationary phase thickness 5 μm), applying temperature programming starting at 50 °C (6 min at the initial temperature) and heating to 260 °C (5 min at the final temperature) at a rate of 15 °C min$^{-1}$. The isotopic compositions of the retained compounds and the high boiling fraction of the effluent were analyzed by a HP 6890N GC–MS (with MSD 5973, EI 70 eV), with a HP-5MS column [30 m, 0.25 mm i.d., (5%-phenyl)-methylpolysiloxane, stationary phase thickness 0.25 μm]. The following temperature programming was applied: 10 °C min$^{-1}$ from 10 °C (1 min at the initial temperature) to 300 °C (5 min at the final temperature). Hexachloroethane was used as the internal standard for the extracts. Similar analyses for the light effluent compounds were performed on a HP 6890 GC–MS (with MSD 5973, EI 70 eV), with a J&W GasPro column (60 m, 0.32 mm i.d.). The following temperature programming was applied: 20 °C min$^{-1}$ from 10 °C (5 min at the initial temperature) to 200 °C (25 min at the final temperature).

## 3. Results and discussion

### 3.1. Physical characteristics of the catalyst

Powder XRD confirmed that the sample consists of a pure and well crystalline MFI phase. The XRD peak broadening analyses suggests a crystallite size (scattering domain size) larger than 100 nm. SEM showed nonuniformly shaped particles in the size range 0.5–5 μm (average, around 2–3 μm). The BET surface area was 370 m$^2$ g$^{-1}$.

Fig. 1 reports a series of IR spectra (1–9) of the zeolite in the $\nu$(OH) region. Spectrum 1 represents the pretreated zeolite before CO adsorption, whereas spectra 2–9 were recorded at increasing CO pressures at −213 °C. The inset displays the difference spectra 2′–9′ in the $\nu$(CO) region. The rather large

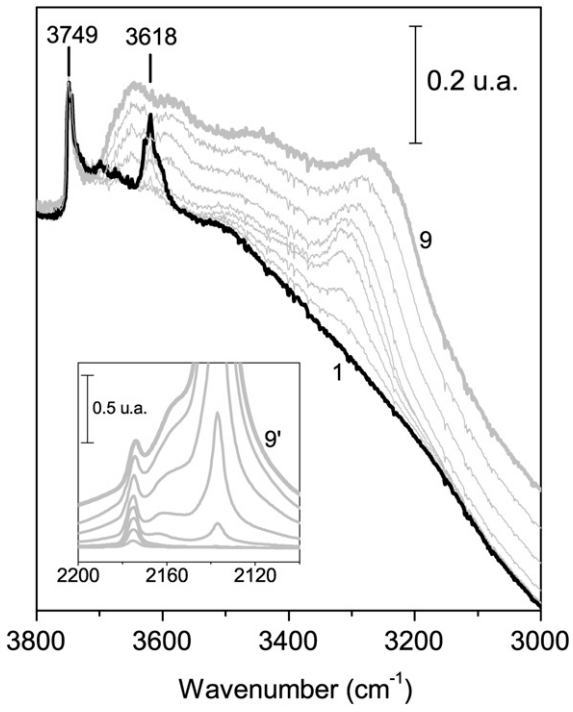


Fig. 1. FTIR spectra of the H-ZSM-5 sample. Spectrum 1 (black) was recorded for the zeolite after outgassing at 500 °C. Spectra 2–9 (gray) were collected at increasing pressures of CO at −213 °C. The inset shows the difference spectra (spectrum 1 subtracted from spectra 2–9) in the $\nu$(CO) region.

crystallite size gives a pronounced scattering background starting at 3000 $cm^{-1}$, and the band associated with the external Si–OH groups (3749 $cm^{-1}$) has a modest intensity. The other general features of the infrared spectrum of the sample are as expected for a zeolite with a relatively low Al content. Two families of OH groups can be clearly distinguished in spectrum 1: (i) isolated Si–OH groups located on the external surface (maximum at 3749 $cm^{-1}$) and in internal defects (low-frequency shoulder/tail on the main band) and (ii) strongly acidic-bridging Si–OH–Al groups in the framework of the zeolite (maximum at 3618 $cm^{-1}$). In addition, a weaker absorption, representing mainly partially hydrolyzed framework Al (expected at around 3660–3680 $cm^{-1}$), can be discerned between these two components. $\nu$(OH) vibrations of extra-framework Al–OH groups, which normally appear at 3782 $cm^{-1}$, cannot be seen for this sample. The acidic strength of these species cannot be assessed by direct measurement of the vibrational frequency of the unperturbed OH groups, but by the shift $\Delta\nu$ caused by the interaction with a basic molecule used as sensitive electric field probe. When adsorbing a base, the observed red shift of the $\nu$(OH) band will be proportional to the Brönsted acidic strength of these species [29–32]. CO is one of the most widely used probe molecules for acidity measurements of zeolites, and extensive data are available [29,33]. Spectra 2–9 show the perturbations induced on the $\nu$(OH) modes at increasing CO pressures. The original $\nu$(OH) modes of the zeolite are gradually consumed while the $\nu$(OH) vibrations of the OH···CO adducts grow in a parallel manner at lower frequencies. The band at 3618 $cm^{-1}$ becomes completely eroded and gives rise to a rather broad band with maximum around 3270 $cm^{-1}$ ($\Delta\nu$(OH) = −350 $cm^{-1}$). The Si–OH groups are partially consumed and shifted to 3645 $cm^{-1}$ ($\Delta\nu$(OH) = −100 $cm^{-1}$). Formation of the OH···CO adducts is also accompanied by a perturbation of the internal vibrational mode of CO. The perturbation of the $\nu$(CO) mode is displayed in the inset. Starting from low coverage, three components are visible at 2137, 2163, and 2175 $cm^{-1}$. Their respective assignments are free liquid like CO, CO adsorbed on weakly acidic Si–OH sites or partially extra-lattice Al–OH, and CO adsorbed on the strongly acidic Brönsted sites. In compliance with the other characterization techniques, these data confirm that the zeolite under study is a representative H-ZSM-5. The low Al content has not increased the acidic strength of the Brönsted sites. This latter observation is important, because it is allows us to consider the mechanistic conclusions of this work to be rather general for H-ZSM-5, not for just one specific sample.

### 3.2. Conversion of methanol over H-ZSM-5

#### 3.2.1. Gas-phase products and retained material at 370 °C and 20 min on stream

At 370 °C, the conversion was 85% (dimethyl ether [DME] included in reactants) over the fresh zeolite (time on stream = 20 min), and the main products were propene, butenes, and various $C_5$–$C_{10}$ hydrocarbons. The detailed composition of the effluent, which is typical for siliceous H-ZSM-5 at these conditions, is shown in Table 1.

Table 1
Product selectivities (C%) and methanol/dimethyl ether conversion (%) at 370 °C

| TOS (min) | Conv. | $C_1$ | $C_2$ | $C_3$ | $C_{4=}$ | $C_{4-}$ | $C_5$ | $C_{6+}$ |
|---|---|---|---|---|---|---|---|---|
| 10 | 85.0 | 0.2 | 6.1 | 32.8 | 16.6 | 5.7 | 13.4 | 25.2 |
| 15 | 84.9 | 0.2 | 6.2 | 32.9 | 16.8 | 5.5 | 13.3 | 25.1 |
| 20 | 84.4 | 0.2 | 6.2 | 32.5 | 16.5 | 5.5 | 13.2 | 25.9 |
| 30 | 85.4 | 0.2 | 6.0 | 32.3 | 16.5 | 5.3 | 13.4 | 26.3 |
| 60 | 85.1 | 0.2 | 6.2 | 33.0 | 16.9 | 5.3 | 13.0 | 25.4 |
| 1200 (20 h) | 82.5 | 0.2 | 7.1 | 32.9 | 16.6 | 5.2 | 12.8 | 25.2 |
| 20160 (14 days) | 10.8 | 1.2 | 10.2 | 34.0 | 20.6 | 3.0 | 12.0 | 19.0 |

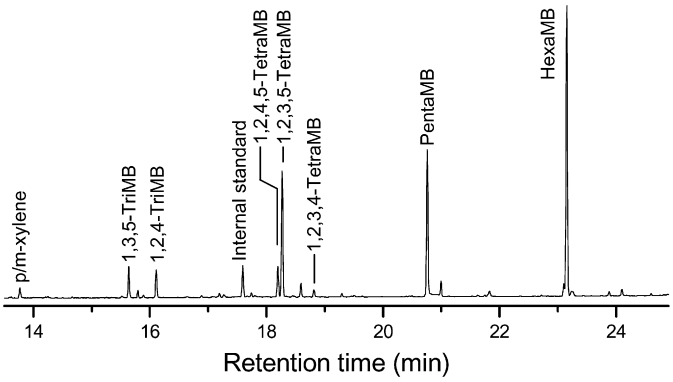


Fig. 2. GC–MS analysis of retained material after 20 min of methanol conversion at 370 °C.

In this report, main attention is given to the buildup and stability of the organic material in the zeolite pores during the reaction. Fig. 2 presents the GC–MS total ion chromatogram of the organics present inside the zeolite after 20 min of methanol reaction at 370 °C. The chromatogram in Fig. 2 was obtained by thermally quenching at 20 min on stream, dissolving the zeolite framework in HF, extracting the organic material with $CH_2Cl_2$, and finally analyzing this extract. As Fig. 2 shows, a few compounds are dominant among the retained organics, and virtually all peaks represent polymethylbenzenes (polyMBs). Hexamethylbenzene (hexaMB) is most abundant, followed by pentamethylbenzene (pentaMB), tetramethylbenzenes (tetraMBs), trimethylbenzenes (triMBs), and *p*/*m*-xylene. Hydrocarbons with greater molecular mass than hexaMB were not present in appreciable amounts. (This is not due to an experimental limitation, because the setup allows analysis of compounds as least as heavy as methylpyrene.) PolyMBs up to tetraMB were also detected in the gas phase; thus, to be precise, only penta- and hexaMB can be considered truly trapped species in this context. Previous studies on the organics formed inside wide-pore zeolites/zeotypes (H-beta and H-SAPO-34) under MTH conditions have shown similar results [15,21], but two essential differences should be underlined:

1. The well-defined cutoff in the distribution of confined organics at hexaMB (Fig. 2) must be a result of the restricted space in the channels of ZSM-5, because far larger polyaromatics are found in copious amounts in zeolites/zeotypes

providing more spacious voids. This point is further corroborated in Section 3.2.2.

2. The accumulation of hexaMB in the zeolite cavities at this rather high temperature (and conversion) points to a low reactivity of this species. This is in stark contrast to the aforementioned investigations in which hexaMB [15] (and heptaMB$^+$) [21] were found to be highly unstable and present in only minute amounts above 325 °C.

### 3.2.2. Retained material at increasing time on stream at 370 °C

Fig. 2 shows that traditional coke-like compounds (polyaromatics) cannot be found in H-ZSM-5 during the MTH reaction, at least not after 20 min of reaction. This may be due to steric limitations or, alternatively, an insufficiently long reaction time (20 min) to allow the buildup of appreciable amounts of polyaromatics. To clarify this, a series of experiments with an extended reaction time (from 10 min to 14 days) were performed. Analyses of the gas-phase products were carried out in parallel to the HF dissolution experiments. The results, given in Table 1, show that a conversion of about 85% was maintained for several hours, but that it dropped to 82.5% after 20 h on stream. After 14 days of reaction, the conversion decreased to 10.8%, and the low activity of the zeolite was accompanied by a lower hydride transfer activity, as reflected in the lower $C_{6+}$ selectivity (less aromatics) and the higher alkene/alkane ratio in, for example, the $C_4$ fraction.

Fig. 3 shows the GC–MS details of the $CH_2Cl_2$ extracts obtained at the same reaction times as those given in Table 1. The concentration of all polyMBs increased consistently up to 20 h. The concentration of hexaMB increased by a factor 3.3 when the reaction time was increased from 10 min to 20 h. The corresponding factors for the lower polyMBs were 1.1 for *p*/*m*-xylene, 1.3 for the triMBs, 1.2–1.7 for the tetraMBs (isomer-dependent), and 1.9 for pentaMB. All methylbenzenes attained a steady-state concentration after 60 min on stream except hexaMB, which increased by a factor of 1.3 from 60 min to 20 h. This suggests that methylation of pentaMB into hexaMB is sterically restricted, because complete methylation is thermodynamically favored.

The changes in absolute and relative concentrations of the organics in the zeolite channels observed during the first 60 min of reaction did not affect the effluent composition. By increasing the reaction time to 20 h, the conversion dropped slightly, with the only change seen in the confined material an increase in hexaMB. However, the increased amount of hexaMB in the zeolite cannot be related to the conversion drop, because the 14-day experiment (Fig. 3) ruled out any correlation between the concentration of organics in the pores and the zeolite deactivation. It is also interesting to note that despite the fact that the catalyst suffered from severe deactivation after 14 days on stream, no larger aromatics were found. Thus, deactivation must result from the formation of large graphitic species (not soluble in $CH_2Cl_2$) on the external surface of the crystallites. This is in strong contrast to the zeolites/zeotypes with more spacious cavities in which coke is readily formed, resulting in rapid deactivation. This is borne out in Fig. 4, which shows the

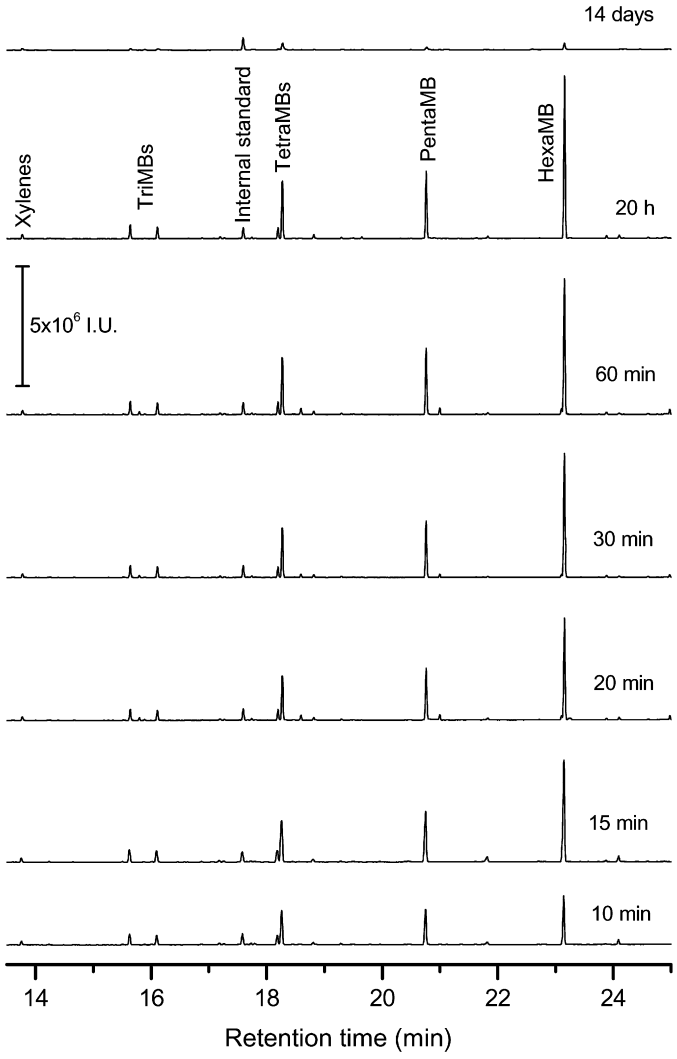


Fig. 3. GC–MS analyses of retained material after methanol conversion at 370 °C.

organic constituents (isolated after HF dissolution) of a deactivated H-SAPO-34. The experiment was conducted at 350 °C, and the distribution of retained organics spanned benzene to methylpyrenes, with different methylated naphthalene isomers as the prevailing species. The concentration of organics in the deactivated H-SAPO-34 is orders of magnitude higher than that found for H-ZSM-5.

A study in progress, specifically devoted to coke formation on H-ZSM-5, has shown a considerable discrepancy between the total coke content determined by temperature programmed oxidation and the mass of the confined organics determined by HF dissolution for a deactivated H-ZSM-5 (Si/Al = 45): The total coke content of the deactivated sample was 28% by mass, whereas the material isolated after HF dissolution constituted only about 0.08% of the total mass of the spent catalyst. This finding indicates that virtually all of the carbon present on a deactivated H-ZSM-5 is insoluble in $CH_2Cl_2$ and thus is of graphitic character.

Behrsing et al. investigated coke formation from methanol over H-ZSM-5 (with Al content ranging from 0.7 to 2.7%

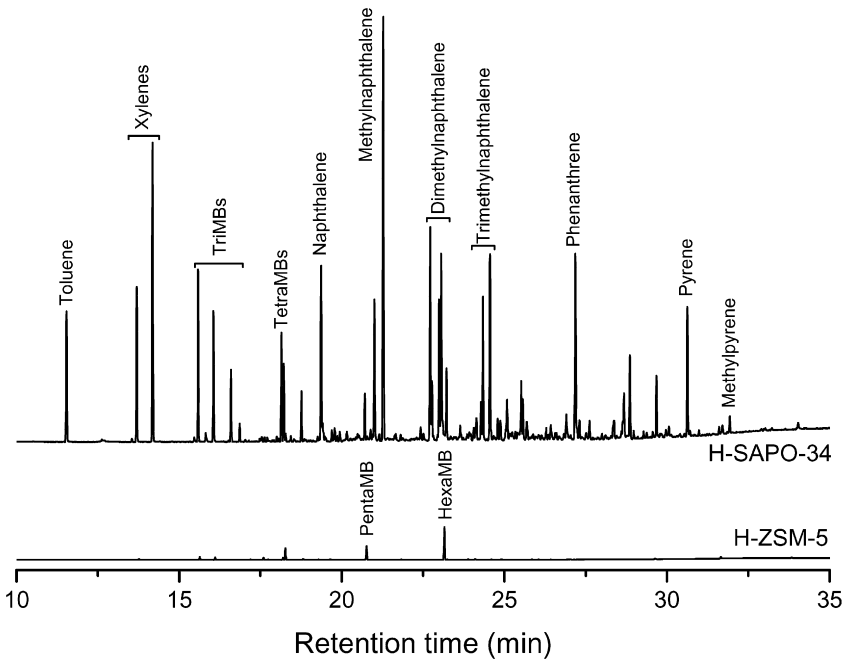


Fig. 4. GC–MS analyses of retained material in severely deactivated H-SAPO-34 (top) and H-ZSM-5 (bottom). The intensity scales are directly comparable.

w/w) using transmission electron microscopy (TEM) and found that the catalysts became deactivated only when the coke deposits contained packets of aromatic sheets of carbon parallel to the catalyst surface [34]. Similar results, also in line with our conclusions, were reached by Gallezot et al. in a study in which *n*-heptane was reacted over H-ZSM-5 [35]. TEM and electron energy loss spectroscopic measurements revealed that the coke was formed as envelopes around the zeolite crystals.

The current data strongly suggest that an all-dominating external coking of H-ZSM-5 explains the superior lifetime properties of this catalyst. We should address the general validity of this statement, because it is well known that the process of coke formation (i.e., cyclization and hydrogen transfer reactions) is closely related to the acidic site density of the zeolite. The present sample has a rather low Al content (Si/Al = 140), implying slow aromatization reactions. But we carried out experiments for H-ZSM-5 samples with Si/Al ratios as low as 25 and found that the overall picture did not seem to change dramatically; no additional compounds (e.g., aromatics larger than hexaMB) appeared, even though the relative and absolute concentrations of the confined organics differed somewhat. A more comprehensive study involving a broader selection of ZSM-5 samples is currently in progress.

### 3.2.3. Retained material after 20 min on stream at 290–390 °C

A previous study found that it was necessary to reduce the reaction temperature to 300 °C to observe the most reactive retained species in the beta zeolite during the MTH reaction [21]. In that case, heptaMB$^+$ (isolated as its corresponding base 1,2,3,3,4,5-hexamethyl-6-methylene-1,4-cyclohexadiene after HF dissolution and extraction) was the dominant compound in the zeolite pores at the lower temperatures, but was hardly observable above 300 °C due to rapid decomposition into alkenes and lower polyMBs. Consequently, we conducted a temperature series for ZSM-5 to observe possible species that are too reactive to be seen at more realistic temperatures. Effluent analyses were carried out in parallel at the different reactor temperatures (Table 2), and the reaction was stopped and the zeolite dissolved in HF after 20 min on stream. Table 2 shows that at the lowest temperature, the conversion was close to zero (0.003%), and the only detectable products were ethene and propene. At the highest temperature (390 °C), the conversion increased to 91%.

Table 2
Product selectivities (C%) and methanol/dimethyl ether conversion (%) at 20 min on steam

| Temp. (°C) | Conv. | $C_1$ | $C_2$ | $C_3$ | $C_{4=}$ | $C_{4-}$ | $C_5$ | $C_{6+}$ |
|---|---|---|---|---|---|---|---|---|
| 290 | 0.003 | 0.0 | 44.0 | 56.0 | 0.0 | 0.0 | 0.0 | 0.0 |
| 310 | 4.8 | 0.5 | 17.5 | 33.2 | 17.8 | 8.4 | 9.3 | 13.4 |
| 330 | 51.6 | 0.2 | 13.7 | 29.7 | 12.4 | 5.1 | 10.2 | 28.7 |
| 350 | 73.0 | 0.2 | 9.9 | 30.4 | 14.3 | 5.2 | 11.7 | 28.4 |
| 370 | 84.9 | 0.2 | 6.2 | 32.9 | 16.8 | 5.5 | 13.3 | 25.1 |
| 390 | 91.0 | 0.2 | 4.8 | 34.5 | 17.4 | 5.2 | 13.9 | 24.0 |

Fig. 5 presents the composition of the retained material formed after 20 min of reaction at the different temperatures. Note that the chromatogram representing experiment conducted at 290 °C is shown at higher (10×) sensitivity. At 290 °C, the concentration of retained organics was very low, and pentaMB seemed to dominate, whereas triMBs can hardly be discerned. Increasing the temperature to 310 °C gave a methanol conversion of 4.8% and orders-of-magnitude increases in the concentrations of the organic material in the zeolite pores. Methanol conversion increased to 51.6% with a further temperature in-

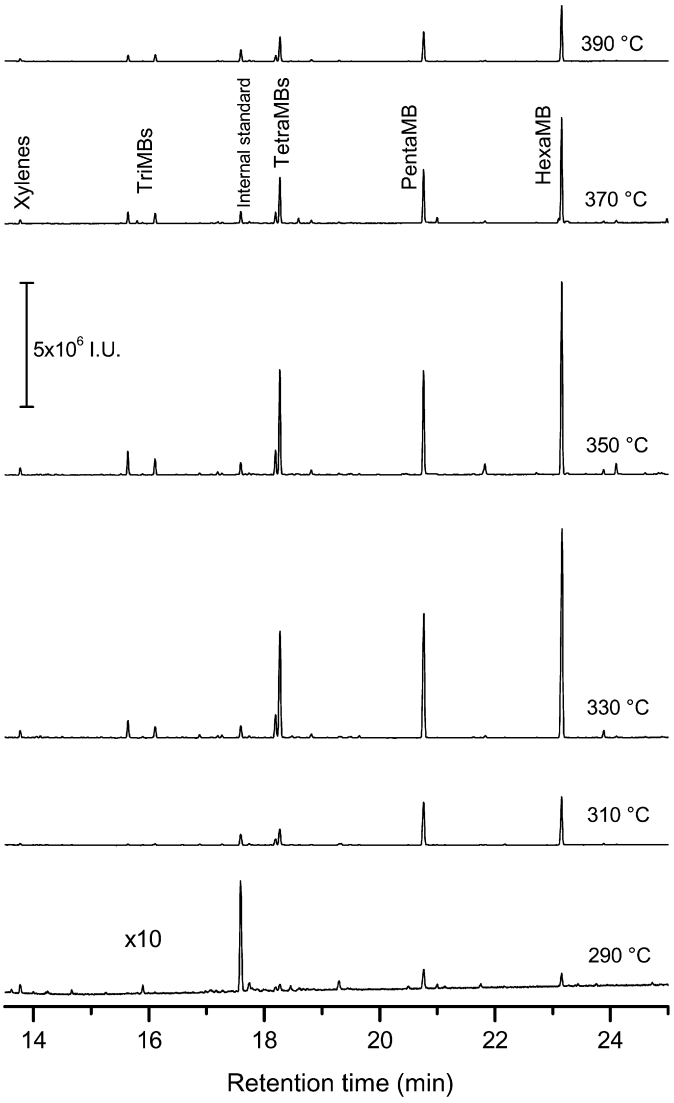


Fig. 5. GC–MS analyses of retained material after 20 min of methanol conversion.

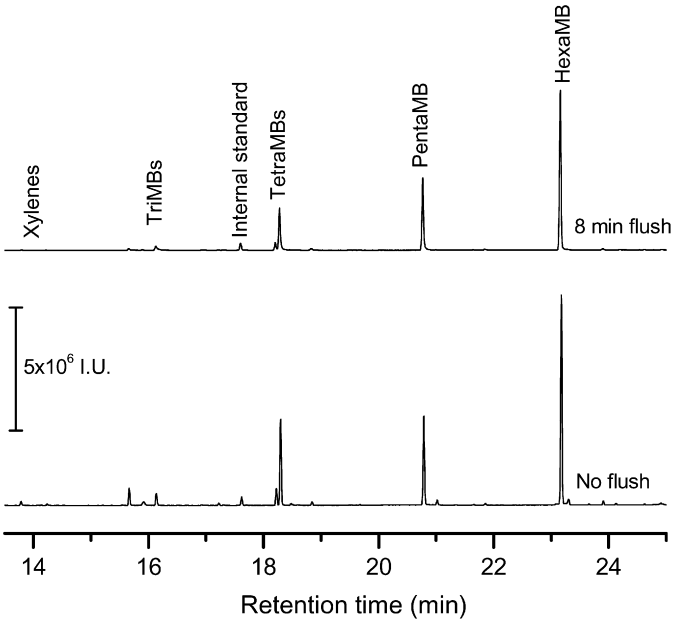


Fig. 6. GC–MS analyses of retained material after 20 min of methanol conversion at 370 °C (bottom) and 20 min of reaction followed by 8 min of flushing with carrier gas at 370 °C.

crease to 330 °C; the temperature rise had the most pronounced effect on the 1,3,5-triMB concentration, which was increased by a factor of 14. The concentrations of the remaining compounds increased in the order 1,2,4-triMB > 1,2,3,5-tetraMB > *p*/*m*-xylene > hexaMB > 1,2,4,5-tetraMB > pentaMB. The concentration of the retained material seemed to reach a maximum between 330 and 350 °C. A further increase in temperature led to lower concentrations of all hydrocarbons in the zeolite channels. Note that the concentration of 1,3,5-triMB suffered more than that of the 1,2,4-isomer in this temperature regime.

It now can be stated that no new possible intermediates or heptaMB$^+$ appeared at lower temperatures, and a reaction route similar to the previously suggested mechanism based on heptaMB$^+$ is not likely to be valid for H-ZSM-5. Obviously, the channels were too narrow to allow the terminal methylation step in which hexaMB forms heptaMB$^+$. The previously mentioned restricted methylation of pentaMB into hexaMB further supports this conclusion.

### *3.2.4. Stability of the retained organic material: Flushing with carrier gas at 350 °C*

To obtain information on the stability of the confined hydrocarbons, an experiment was carried out in which the feed was stopped after 20 min of reaction and the catalyst was flushed with carrier gas for 2, 4, and 8 min at the reaction temperature. Fig. 6 shows the effect of catalyst flushing on the hydrocarbon deposits by comparing the analysis from the 8-min flushing experiment with that obtained after 20 min of reaction. In view of what we have learned from other zeolites, the results are rather surprising. Similar experiments on H-beta and H-SAPO-34, but at a considerably lower reaction temperature (325 °C), led to a total disappearance of hexaMB at 1–2 min after methanol cutoff [15,18].

On flushing, the polyMBs disappeared from the zeolite channels at rates according to the following order: *p*/*m*-xylene > 1,3,5-triMB > 1,2,4-triMB > 1,2,4,5-tetraMB > 1,2,3,5-tetraMB > pentaMB = hexaMB.

On the basis of the findings of the flushing experiment, we can draw the following conclusions:

1. Penta- and hexaMB have a similar decomposition rate after methanol cutoff, provided that their diffusion rates are equal (zero).
2. Penta- and hexaMB show very slow decomposition rates in the zeolite compared with those found for other zeolites/zeotypes [15,18].
3. The tetraMBs are very persistent during flushing.
4. Apparently, 1,3,5-triMB disappears faster than the 1,2,4-isomer. This is opposite to what would be expected from the relative diffusion rates, because 1,3,5-triMB is the most sterically demanding. The explanation for this finding could be that 1,3,5-triMB decomposes rapidly, or simply

that 1,3,5-triMB isomerizes into 1,2,4-triMB, which then diffuses out of the zeolite crystals.

Indeed, we should mention that the observed slow decomposition of penta- and hexaMB during the flushing experiment does not necessarily imply low reactivity in the working zeolite. After several minutes of flushing, the concentration of methanol in the pores is low, and the slow decomposition of penta- and hexaMB may not reflect their reactivity in the presence of methanol. The reactivity of the different retained species in the presence of methanol is further corroborated in the next section.

### 3.2.5. Switching to $^{13}C$ methanol after having built up organics from $^{12}C$ methanol: rate of $^{13}C$ incorporation in the retained organic material and gas phase products

To assess the reactivity patterns of the confined organics toward methanol (i.e., toward the reactant) in the working catalyst, a series of experiments were conducted in which ordinary $^{12}C$ methanol was reacted for 18 min followed by a rapid switch to $^{13}C$ methanol feed, reacted for a shorter time (0.5, 1, or 2 min). The compositions of both retained material and effluent were practically the same in all three experiments—the same as that shown for 20 min on stream in Fig. 5 and Table 2, respectively. Isotopic analysis of both the retained material and the gas-phase products was performed after 0.5, 1, and 2 min of $^{13}C$ methanol reaction.

*3.2.5.1. Retained material* Fig. 7 shows isotopic data for the material isolated after dissolving the used catalyst with HF and extracting with $CH_2Cl_2$. Panel (a) displays the isotopomer distributions for the three different $^{13}C$ methanol reaction times; panel (b) shows the time developments of the total $^{13}C$ contents in the different molecules. Clearly, there are large differences in both $^{13}C$ distributions and total content among the various compounds. Further, Fig. 7 shows an evident trend for the higher methylbenzenes: The incorporation of $^{13}C$ consistently slows as the number of methyl substituents increases. After 0.5 min of $^{13}C$ methanol reaction, xylenes and triMBs display broad distributions centered around the isotopomers that are highly rich in $^{13}C$. The tetraMB isotopomers are also broadly distributed, but the molecules that do not contain any $^{13}C$ are the most abundant. This latter observation is even more pronounced for pentaMB and in particular for hexaMB. After 1 and 2 min of $^{13}C$ methanol reaction, the distributions for the lower methylbenzenes are skewed toward complete $^{13}C$ incorporation, and the distributions become bimodal for the tetraMBs and pentaMB, whereas hexaMB remains dominated by isotopomers not containing $^{13}C$. The total $^{13}C$ contents displayed in Fig. 7 also reflect the trend in reactivity among the retained methylbenzenes. Similar isotope experiments conducted for the H-SAPO-34 [14] and H-beta [21] catalysts have shown the reverse trend, with hexaMB having the highest rate of $^{13}C$ incorporation.

Two minor points regarding the methylbenzene isomers also should be mentioned. In the flushing experiment (discussed in Section 3.2.4), 1,3,5-triMB disappeared faster than 1,2,4-triMB after methanol cutoff; however, identical isotopic data were obtained for the two retained triMB isomers (Fig. 7), which strongly disfavors any differences in reactivity. In contrast, for the two tetraMB isomers, the isotopic distributions and total $^{13}C$ contents differed significantly. At 0.5 min of $^{13}C$ methanol reaction, 1,2,4,5-tetraMB contained 40% labeled carbons, whereas 1,2,3,5-tetraMB contained 52%. An explanation for these differences is not apparent, but 1,2,3,5-tetraMB is somewhat bulkier than 1,2,4,5-tetraMB and thus will reside within the zeolite channels for a longer time. Indeed, only 1,2,4,5-tetraMB is present in appreciable amounts in the effluent. However, as a whole, the behavior of both tetraMB isomers is consistent with the general trend of a decreasing rate of $^{13}C$ incorporation with an increasing the number of methyl groups.

*3.2.5.2. Gas-phase products* The isotopic compositions of the effluent compounds were also determined after 0.5, 1, and 2 min of $^{13}C$ methanol reaction; the data thus obtained are shown in Fig. 8. Some compounds are present both in the effluent and the retained material, that is, *p*/*m*-xylene, 1,2,4-triMB, and 1,2,4,5-tetraMB. The trend for these compounds seen in the retained material is lost in the effluent. The data for *p*/*m*-xylene and 1,2,4-triMB are fairly similar in both the retained material and the effluent, but 1,2,4,5-tetraMB is considerably richer in $^{13}C$ in the gas phase. In fact, in the gas phase, the $^{13}C$ content of 1,2,4,5-tetraMB is very similar to that seen for *p*/*m*-xylene and 1,2,4-triMB.

For all effluent compounds, the $^{13}C$ methanol exchange is fairly rapid (Fig. 8), but some important differences, particularly evident at short $^{13}C$ reaction times, have valuable mechanistic implications. Based on the data in Fig. 8, the compounds may be divided into two groups: The rates of $^{13}C$ incorporation are significantly slower for ethene and the aromatics compared with the $C_3$–$C_6$ alkenes. This is reflected in the isotopomer distributions for ethene and the aromatics, which are broader than those observed for the $C_3$–$C_6$ alkenes, in the sense that the pure $^{13}C$ isotopomers are more dominant for the latter group. The grouping is even more striking when comparing the time developments in the total $^{13}C$ content. For the sake of clarity, Fig. 9 collects these data in a single plot for all compounds. Clearly, the $C_3$–$C_6$ alkenes are systematically richer in $^{13}C$ than ethene and the aromatics, and the $^{13}C$ contents virtually overlap within the two compound groups. These results suggest a mechanistic link between the ethene formation and the aromatics in the effluent. Moreover, the significantly higher $^{13}C$ content in the $C_3$–$C_6$ alkenes suggests a different or additional route for methanol incorporation into these compounds.

## 3.3. Reaction mechanism for the MTH reaction over H-ZSM-5

In this report we have shown that methylbenzenes up to and including hexaMB are present in copious amounts in H-ZSM-5 during the MTH reaction. Isolated, this finding is in accord with similar investigations of other related catalysts. However, in stark contrast to all previous conclusions [13–15,18,21], the highest methylbenzenes do not appear to play a significant part in the mechanism for alkene formation. PentaMB and hexaMB are present in the working zeolite at realistic reaction temperatures, contradictory to the expected behavior of a reactive in-

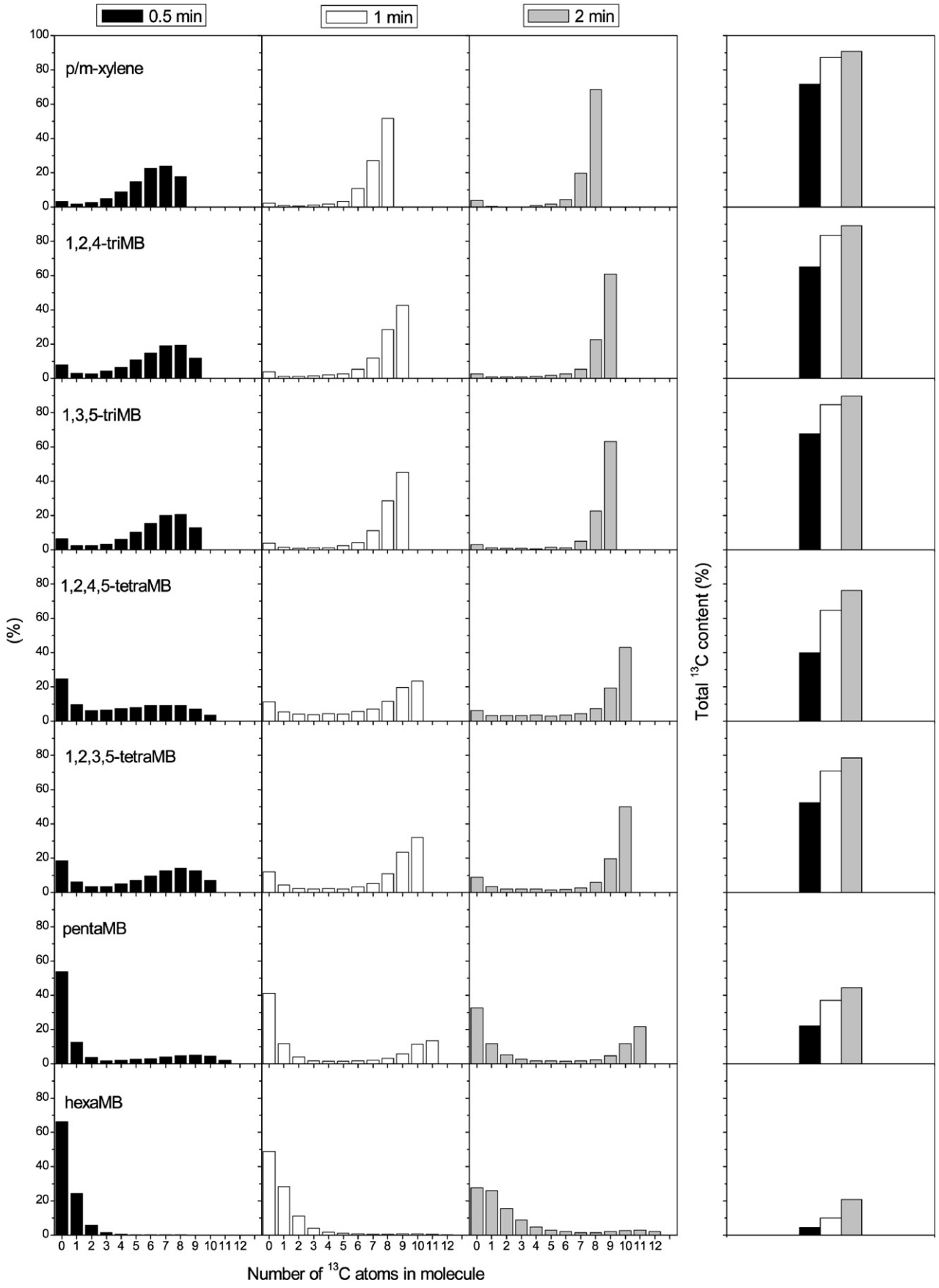


Fig. 7. Isotopic distributions (panel a, left) and total $^{13}$C content (panel b, right) in retained organic material after 18 min of $^{12}$C methanol reaction followed by a switch to $^{13}$C methanol at 350 °C. $^{13}$C methanol was reacted for 0.5 min (black bars), 1 min (white bars), and 2 min (gray bars) after $^{12}$C methanol reaction.

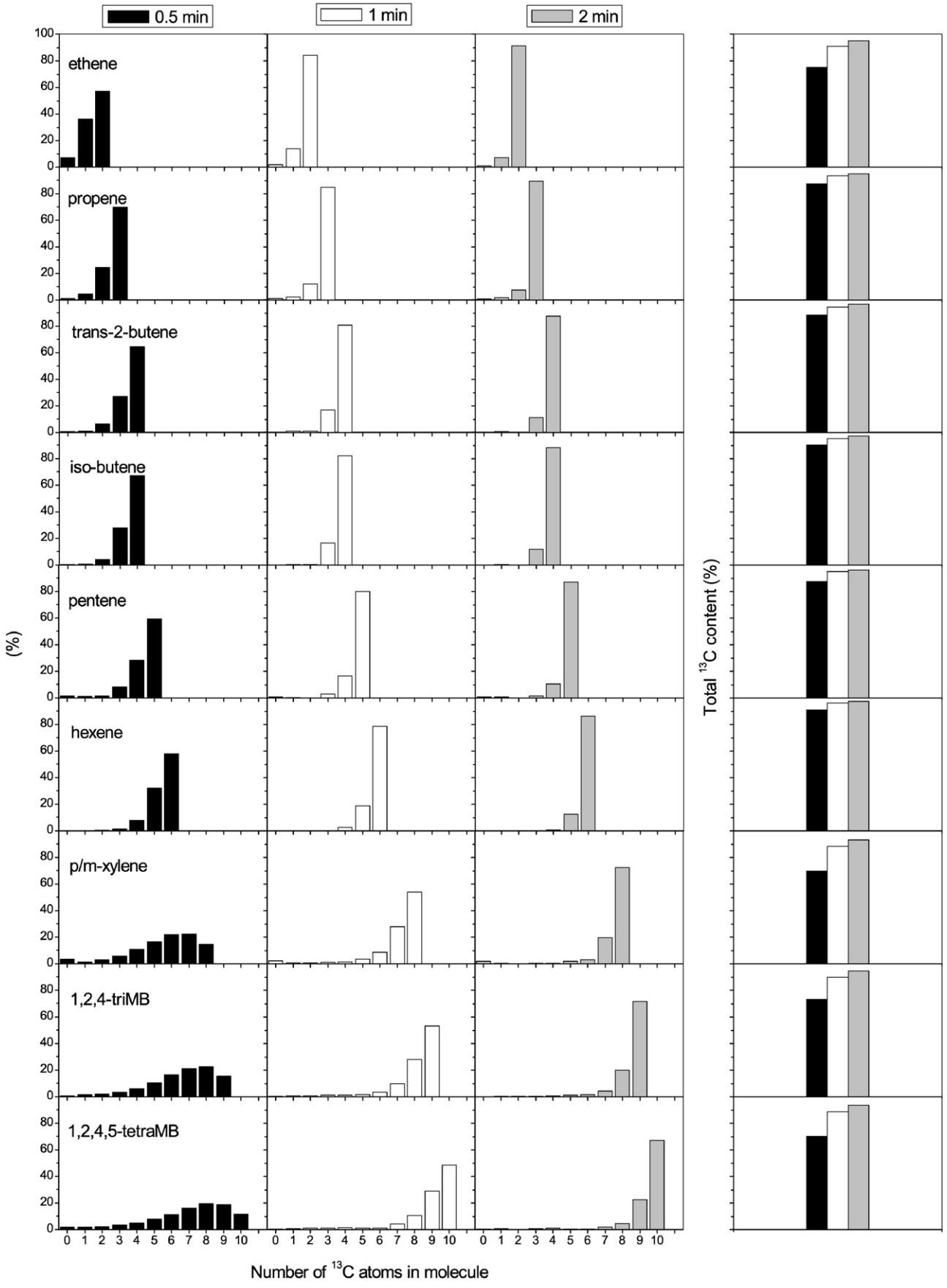


Fig. 8. Isotopic distributions (panel a, left) and total $^{13}C$ content (panel b, right) in the effluent compounds after 18 min of $^{12}C$ methanol reaction followed by a switch to $^{13}C$ methanol at 350 °C. $^{13}C$ methanol was reacted for 0.5 min (black bars), 1 min (white bars), and 2 min (gray bars) after $^{12}C$ methanol reaction.

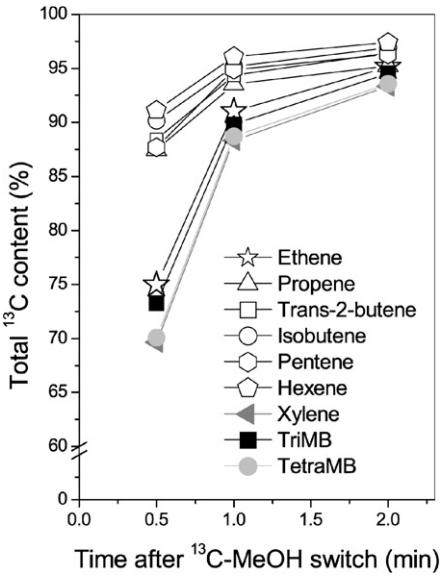


Fig. 9. Total $^{13}$C content in the effluent compounds after 18 min of $^{12}$C methanol reaction followed by a switch to $^{13}$C methanol and further reaction for 0.5, 1.0, and 2.0 min at 350 °C. Note the scale break.

termediate, and are also stable during flushing after methanol cutoff at 350 °C. In addition, the isotope data decisively confirm that, compared with the lower methylbenzenes, pentaMB and hexaMB are inert toward methanol. Finally, heptaMB$^+$ was not observed, despite the broad range of reaction conditions studied. As a direct implication, a hydrocarbon pool mechanism involving the highest methylbenzenes or heptaMB$^+$, proven to be dominant for H-beta and H-SAPO-34 [14,15,18,21], cannot be responsible for any appreciable activity in the H-ZSM-5 catalyst.

However, the data suggest that a hydrocarbon pool mechanism involving the xylenes and triMB as the reactive intermediate operates over H-ZSM-5. Based on the practically identical $^{13}$C contents and time evolutions (Fig. 9), ethene appears to be formed predominantly via the xylenes and/or the triMBs. The $C_3$–$C_6$ alkenes do not display this clear correspondence with any of the polymethylbenzenes. Haw and co-workers [23,36] have indeed shown that the lower methylbenzenes may split off mainly ethene and that the higher analogues yield predominantly propene. It is not possible to assess the exact mechanism by which ethene is lost from the pool compounds from the current data, but several relevant suggestions exist in the literature. In experiments where $^{13}$C methanol was co-reacted with benzene or toluene at steady state conditions over H-ZSM-5, Mikkelsen et al. [12] observed a relation between the methylbenzenes and both ethene and propene formation. In one case where $^{12}$C benzene and $^{13}$C methanol were co-reacted, the ethene thus formed contained significantly less $^{13}$C than propene, suggesting that a larger fraction of the ethene relative to propene was formed via methylbenzenes. This is in compliance with our results. However, when $^{12}$C toluene and $^{13}$C methanol were co-reacted, no significant distinction between ethene and propene could be made.

Based on these observations, it seems reasonable to assume that a fraction of the propene is formed from the aromatics. Pinpointing the exact extent of propene formation via this route is the aim of further studies already in progress. It should be pointed out, however, that the addition of large amounts of a reactant (benzene/toluene) in addition to methanol might lead to results less general in nature. The present data do not suffer from the perturbation that a co-reactant may induce, because methanol is the only reactant in all experiments.

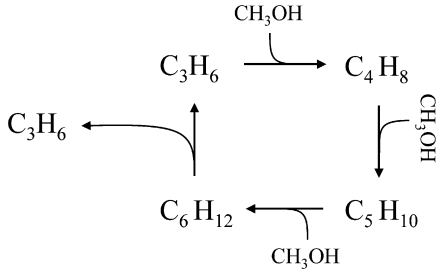


Scheme 2. Suggested mechanism for propene formation via the alkene cracking/methylation route.

The $C_3$–$C_6$ alkenes contain more $^{13}$C than all other products. This enrichment must be attributed to $^{13}$C incorporation by another mechanism, not viable for ethene, and the only satisfactory explanation is an alkene methylation reaction. Kinetic investigations have shown that ethene methylation is between one and two orders of magnitude slower than for propene and linear butanes [37,38]; this has been further supported by quantum chemical studies [39]. Thus, ethene methylation is a very minor reaction under the current set of reaction conditions. It thus seems very probable that additional $^{13}$C is introduced into the $C_3$–$C_6$ alkenes via repeated methylations, and that the carbon atoms are distributed among the product fractions through subsequent cracking steps. Such a sequence of reactions, illustrating how three molecules of methanol are converted into propene, is outlined in Scheme 2. In this scheme, the reaction cycle starts with propene and ends up with hexene cracked into two molecules of propene. This is, of course, a simplification, because far larger alkenes may be formed before they are cracked, and the cracking products may be alkenes higher than propene. Dimerization also might occur, but this will not lead to additional $^{13}$C incorporation.

As was the case for methylation, ethene dimerization is also slow compared with that of propene and butenes [40]. The importance of alkene methylation and cracking in the MTH reaction was recognized early and pointed out in particular by Dessau and co-workers at Mobil Oil [41]. In the original methylation/cracking reaction schemes, however, ethene was included, even though its slow formation through cracking was emphasized. Indeed, in the cracking of 3,4-dimethyl-3-hexene over the Y zeolite at 350 °C, the molar yields for propene and butenes have been shown to be 14 and 33 times higher than the yield of ethene [42]. Dessau [41] unsatisfactorily concluded that ethene was formed by a secondary re-equilibration of primary alkenes. This is not in agreement with our findings, because the discrepancy between the $^{13}$C content in ethene and the $C_3$–$C_6$ alkenes excludes any measurable ethene formation from the higher alkenes, however secondary in nature. It should be noted that based on the current level of mechanis-

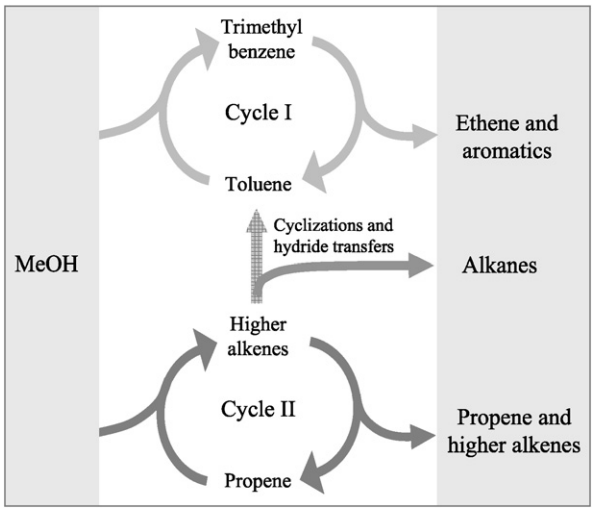


Scheme 3. Suggested dual cycle concept for the conversion of methanol over H-ZSM-5.

tic insight, in particular the shift of focus from coupling of $C_1$ units (methanol/dimethyl ether) to the more indirect hydrocarbon pool mechanism, the designation of products as "primary" or "secondary" often leads to confusion rather than clarification. Clearly, the reactant molecules (methanol) undergo many reaction steps before the formation of even the simplest C–C bond containing product in the zeolite voids.

Based on the present results, it can be established that two mechanistic cycles run simultaneously during the MTH reaction over H-ZSM-5: ethene formation from the lower methylbenzenes followed by remethylation, and a methylation/cracking cycle involving only the $C_{3+}$ alkenes. This is depicted in Scheme 3. Cycle I in Scheme 3 is the aromatics/ethene (with aromatics formally represented by toluene and trimethylbenzene) cycle, whereas cycle II is the alkene-based cycle. A highly interesting question regarding both mechanistic understanding and selectivity control is whether cycles I and II operate completely independently or if they are intertwined in some manner. According to our results, a completely independent operation can hardly be the case for H-ZSM-5. There is a continuous production of aromatics during the reaction; hence there must be a corresponding aromatization of higher alkenes formed in cycle II. This implies that cycle I cannot run without cycle II over H-ZSM-5. However, the two cycles might not be mutually dependent. Based on the low reactivity of ethene toward methanol relative to that of propene and butenes mentioned above, the contribution to the $C_3$–$C_6$ alkenes involving ethene is very small and possibly not required. However, the significance of propene formation from the methylbenzenes cannot be evaluated at this point. Even so, for a given catalyst topology or for a given set of conditions, we may imagine that methanol can be converted solely according to cycle II.

## 4. Conclusion

This study has demonstrated that the following occur during the conversion of methanol to hydrocarbons over H-ZSM-5:

1. The higher methylbenzenes (penta- and hexamethylbenzene) are present in the zeolite pores but are virtually unreactive, both with respect to flushing with carrier gas and incorporation of $^{13}C$ after switching from $^{12}C$ to $^{13}C$ methanol feed. This poor reactivity is contrary to observations made for H-beta and H-SAPO-34.
2. Deactivation is not an effect of coke formation inside the zeolite voids. External coking appears to be the only plausible cause of the loss of activity with time on stream, which might explain the outstanding catalytic stability of H-ZSM-5.
3. Ethene displays the same $^{13}C$ content and time evolution as *p*/*m*-xylene and the triMBs after switching and appears to be formed predominantly from the lower methylbenzenes through a modified hydrocarbon pool mechanism.
4. In contrast to ethene, propene and higher alkenes are formed to a considerable extent from alkene methylations and interconversions (e.g., cracking reactions).

The latter two statements, implying that ethene and propene are formed through different routes, are of utmost importance for understanding and possibly controlling the ethene/propene selectivity in MTO/MTP catalysis.

## References

[1] M. Stöcker, Microporous Mesoporous Mater. 29 (1999) 3.
[2] J. Topp-Jørgensen, Stud. Surf. Sci. Catal. 36 (1988) 293.
[3] J.Q. Chen, A. Bozzano, B. Glover, T. Fuglerud, S. Kvisle, Catal. Today 106 (2005) 103.
[4] W. Song, D.M. Marcus, H. Fu, J.O. Ehresmann, J.F. Haw, J. Am. Chem. Soc. 124 (2002) 3844.
[5] D.M. Marcus, K.A. McLachlan, M.A. Wildman, J.O. Ehresmann, P.W. Kletnieks, J.F. Haw, Angew. Chem. Int. Ed. 45 (2006) 3133.
[6] D. Lesthaeghe, V. Van Speybroeck, G.B. Marin, M. Waroquier, Angew. Chem. Int. Ed. 45 (2006) 1714.
[7] W. Wang, A. Buchholz, M. Seiler, M. Hunger, J. Am. Chem. Soc. 125 (2003) 15260.
[8] Y. Jiang, W. Wang, V.R.M. Marthala, J. Huang, B. Sulikowski, M. Hunger, J. Catal. 238 (2006) 21.
[9] I.M. Dahl, S. Kolboe, Catal. Lett. 20 (1993) 329.
[10] I.M. Dahl, S. Kolboe, J. Catal. 149 (1994) 458.
[11] P.W. Goguen, T. Xu, D.H. Barich, T.W. Skloss, W. Song, Z. Wang, J.B. Nicholas, J.F. Haw, J. Am. Chem. Soc. 120 (1998) 2650.
[12] Ø. Mikkelsen, P.O. Rønning, S. Kolboe, Microporous Mesoporous Mater. 40 (2000) 95.
[13] W. Song, J.F. Haw, J.B. Nicholas, C.S. Heneghan, J. Am. Chem. Soc. 122 (2000) 10726.
[14] B. Arstad, S. Kolboe, J. Am. Chem. Soc. 123 (2001) 8137.
[15] B. Arstad, S. Kolboe, Catal. Lett. 71 (2001) 209.
[16] A. Sassi, M.A. Wildman, H.J. Ahn, P. Prasad, J.B. Nicholas, J.F. Haw, J. Phys. Chem. B 106 (2002) 2294.
[17] A. Sassi, M.A. Wildman, J.F. Haw, J. Phys. Chem. B 106 (2002) 8768.
[18] M. Bjørgen, U. Olsbye, S. Kolboe, J. Catal. 215 (2003) 30.
[19] M. Bjørgen, F. Bonino, S. Kolboe, K.-P. Lillerud, A. Zecchina, S. Bordiga, J. Am. Chem. Soc. 125 (2003) 15863.
[20] M. Bjørgen, U. Olsbye, S. Svelle, S. Kolboe, Catal. Lett. 93 (2004) 37.
[21] M. Bjørgen, U. Olsbye, D. Petersen, S. Kolboe, J. Catal. 221 (2004) 1.
[22] S. Svelle, M. Bjørgen, S. Kolboe, D. Kuck, M. Letzel, U. Olsbye, O. Sekiguchi, E. Uggerud, Catal. Lett. 109 (2006) 25.
[23] B. Arstad, J.B. Nicholas, J.F. Haw, J. Am. Chem. Soc. 126 (2004) 2991.
[24] U. Olsbye, M. Bjørgen, S. Svelle, K.-P. Lillerud, S. Kolboe, Catal. Today 106 (2005) 108.

[25] S. Svelle, F. Joensen, J. Nerlov, U. Olsbye, K.-P. Lillerud, S. Kolboe, M. Bjørgen, J. Am. Chem. Soc. 128 (2006) 14770.
[26] G. Spoto, E.N. Gribov, G. Ricchiardi, A. Damin, D. Scarano, S. Bordiga, C. Lamberti, A. Zecchina, Prog. Surf. Sci. 76 (2004) 71.
[27] S. Svelle, U. Olsbye, K.-P. Lillerud, S. Kolboe, M. Bjørgen, J. Am. Chem. Soc. 128 (2006) 5618.
[28] P. Magnoux, P. Roger, C. Canaff, V. Fouche, N.S. Gnep, M. Guisnet, Stud. Surf. Sci. Catal. 34 (1987) 317.
[29] A. Zecchina, S. Bordiga, G. Spoto, Phys. Chem. Chem. Phys. 7 (2005) 1627.
[30] M.A. Makarova, V.L. Zholobenko, K.M. Al-Ghefaili, N.E. Thompson, J. Dewing, J. Dwyer, J. Chem. Soc. Faraday Trans. 90 (1994) 1047.
[31] J.A. Lercher, C. Gründling, G. Eder-Mirth, Catal. Today 27 (1996) 353.
[32] H. Knözinger, S. Huber, J. Chem. Soc. Faraday Trans. 94 (1998) 2047.
[33] M.A. Makarova, A.F. Ojo, K. Karim, M. Hunger, J. Dwyer, J. Phys. Chem. 98 (1994) 3619.
[34] T. Behrsing, H. Jaeger, J.V. Sanders, Appl. Catal. 54 (1988) 289.
[35] P. Gallezot, C. Leclercq, M. Guisnet, P. Magnoux, J. Catal. 114 (1987) 100.
[36] W. Song, H. Fu, J.F. Haw, J. Am. Chem. Soc. 123 (2001) 4749.
[37] S. Svelle, P.O. Rønning, U. Olsbye, S. Kolboe, J. Catal. 234 (2005) 385.
[38] S. Svelle, P.O. Rønning, S. Kolboe, J. Catal. 224 (2004) 115.
[39] S. Svelle, B. Arstad, S. Kolboe, O. Swang, J. Phys. Chem. B 107 (2003) 9281.
[40] S. Svelle, S. Kolboe, O. Swang, J. Phys. Chem. B 108 (2004) 2953.
[41] R.M. Dessau, J. Catal. 99 (1986) 111.
[42] Y.V. Kissin, Catal. Rev. 43 (2001) 85.